Angular momentum in human walking

Hugh Herr[1,2,*] and Marko Popovic[1]

[1]The MIT Media Laboratory and [2]The Harvard-MIT Division of Health Sciences and Technology, 20 Ames Street, Cambridge, MA 02139, USA

*Author for correspondence (e-mail: hherr@media.mit.edu)

SUMMARY

Angular momentum is a conserved physical quantity for isolated systems where no external moments act about a body's center of mass (CM). However, in the case of legged locomotion, where the body interacts with the environment (ground reaction forces), there is no *a priori* reason for this relationship to hold. A key hypothesis in this paper is that angular momentum is highly regulated throughout the walking cycle about all three spatial directions $[|\vec{L}(t)|{\approx}0]$, and therefore horizontal ground reaction forces and the center of pressure trajectory can be explained predominantly through an analysis that assumes zero net moment about the body's CM. Using a 16-segment human model and gait data for 10 study participants, we found that calculated zero-moment forces closely match experimental values (R_x^2=0.91; R_y^2=0.90). Additionally, the centroidal moment pivot (point where a line parallel to the ground reaction force, passing through the CM, intersects the ground) never leaves the ground support base, highlighting how closely the body regulates angular momentum. Principal component analysis was used to examine segmental contributions to whole-body angular momentum. We found that whole-body angular momentum is small, despite substantial segmental momenta, indicating large segment-to-segment cancellations (~95% medio-lateral, ~70% anterior–posterior and ~80% vertical). Specifically, we show that adjacent leg-segment momenta are balanced in the medio-lateral direction (left foot momentum cancels right foot momentum, etc.). Further, pelvis and abdomen momenta are balanced by leg, chest and head momenta in the anterior–posterior direction, and leg momentum is balanced by upper-body momentum in the vertical direction. Finally, we discuss the determinants of gait in the context of these segment-to-segment cancellations of angular momentum.

Key words: biomechanics, biped, locomotion, angular momentum, human.

INTRODUCTION

The advancement of a comprehensive model of human walking is a formidable task and a critical research objective in the fields of biomechanics, neural science and legged machine control. Although many walking studies have put forth experimental and theoretical descriptions of center of mass (CM) mechanics and energetics (Saunders et al., 1953; Bekker, 1956; Alexander, 1976; Cavagna et al., 1976; Margaria, 1976; Mochon and McMahon, 1980a; Mochon and McMahon, 1980b; McGeer, 1990; Lee and Farley, 1998; Croce et al., 2001; Kuo, 2002; Ortega and Farley, 2005; Geyer et al., 2006; Srinivasan and Ruina, 2006), surprisingly few investigations have specifically focused upon whole-body rotational behavior. Clearly, a comprehensive understanding of human walking would require descriptions of not only global body translations but also rotations. The objective of this investigation was to study the rotational behavior of human steady-state walking through the characterization of whole-body angular momentum, as well as body segment momenta, computed about the body's CM.

The preponderance of research into human angular momentum behaviors has focused not on walking but on other movement tasks such as sit-to-stand maneuvers (Riley et al., 1997), running (Hinrichs et al., 1983; Hinrichs, 1982; Hinrichs, 1987; Hinrichs, 1992) and various sporting activities (Frohlich, 1979; Dapena and McDonald, 1989; Dapena, 1978; Dapena, 1993; LeBlanc and Dapena, 1996; King 1999). Specific to walking maneuvers, Elftman (Elftman, 1939) calculated the angular momenta of all body segments across one walking step, from heel strike to toe-off.

Based on pilot data from a single human participant, he argued that the arms reduced both angular momentum and rotation about both vertical and medio-lateral (left–right) axes.

Following Elftman's findings in the late 1930s, it was not until the turn of the century that additional research was conducted in the area of human walking angular momentum behaviors. Xu and Wang (Xu and Wang, 1998) quantified angular momenta for lower-extremity segments for altering direction during walking, and Simoneau and Krebs (Simoneau and Krebs, 2000) studied whole-body angular momentum in elderly participants in an attempt to quantify balance deficiencies in the elderly population. More recently, a pilot study on a single study participant found that whole-body angular momentum is highly regulated about all three spatial directions in walking, not deviating substantially from zero throughout each phase of gait (Popovic et al., 2002; Gu, 2003; Popovic et al., 2004a).

Although angular momentum behaviors have been studied for human walking, the studies have been limited to a single study participant and often a single walking step. In this study we examined angular momentum behaviors of 10 study participants walking at self-selected speeds. Motivated by the findings of previous pilot investigations that showed a relatively small whole-body angular momentum, we hypothesized that horizontal ground reaction forces and the center of pressure (CP) trajectory in steady-state walking can be explained predominantly through an analysis that assumes zero net moment about the body's CM. To test the hypothesis, we first derived what the horizontal ground reaction force, and CP location, would be if no moments were to act about

the body's CM. Using a 16-segment human model and gait data from the 10 study participants, we tested the hypothesis by comparing the calculated zero-moment forces and CP trajectory with measured values from a force platform.

We also examined segmental contributions to whole-body angular momentum. Motivated by Elftman (Elftman, 1939), we hypothesized that whole-body angular momentum is small throughout the walking gait cycle, despite substantial segmental momenta, indicating large segment-to-segment cancellations. Specifically, since the arms and legs alternately protract and retract within the sagittal plane, we anticipated that adjacent limb segment contributions are effectively balanced in the medio-lateral direction. Furthermore, due to pelvic obliquity, where the leg hip that is entering the swing phase drops lower than the adjacent leg hip (Saunders et al., 1953), we hypothesized that angular momenta contributions of the pelvis and abdomen are balanced by contributions from the rest of the body in the anterior–posterior (front–back) direction. Still further, due to pelvic rotation where the pelvis and upper body rotate about the vertical axis over the stance leg in walking (Saunders et al., 1953), we anticipated that leg angular momentum is balanced by upper-body momentum in the vertical direction. To test these hypotheses, we once again employed the 16-segment human model and gait data measured from the 10 study participants. Principal component (PC) analysis was performed on all 16 body segments' angular momenta to produce PCs for each of three orthogonal directions. We then calculated their respective time-dependent weighting coefficients, or tuning coefficients. Finally, we obtained the amount and source of segmental momentum cancellation for all three spatial directions.

MATERIALS AND METHODS
Experimental procedures
Kinetic and kinematic walking data were collected at the Gait Laboratory of Spaulding Rehabilitation Hospital, Harvard Medical School, in a study approved by the Spaulding committee on the Use of Humans as Experimental Subjects. Ten healthy adult participants, five male and five female, with an age range from 20 to 38 years, volunteered for the study. The participants walked at a self-selected speed across a 10 m walkway in the Motion Analysis Laboratory. Participants were timed between two fixed points to ensure that the same walking speed was used between experimental trials. Walking speeds within a ±5% interval from the self-selected speed were accepted. For each study participant, a total of seven walking trials were collected.

The data collection procedures were based on standard techniques (Kadaba et al., 1989; Winter, 1990; Kadaba et al., 1990; Kerrigan et al., 2000; Kerrigan et al., 2001). An infrared camera system (eight cameras, VICON 512 motion analysis system, Oxford Metrics, Oxford, UK) was used to measure the three-dimensional locations of reflective markers at 120 frames s^{-1}. A total of 33 markers were placed on various parts of a participant's body: 16 lower-body markers, five trunk markers, eight upper-limb markers and four head markers. The markers were attached to the following bony landmarks: bilateral anterior superior iliac spines, posterior superior iliac spines, lateral femoral condyles, lateral malleoli, forefeet and heels. Additional markers were rigidly attached to wands over the mid-femur and mid-shaft of the tibia. The kinematics of the upper body were also collected with markers placed on the following locations: sternum, clavicle, C7 vertebra, T10 vertebra, head, and bilaterally on the shoulder, elbow and wrist. The VICON 512 system was able to detect marker position with a precision of ~1 mm.

During the walking trials, ground reaction forces were measured synchronously with the kinematic data at a sampling rate of 1080 Hz using two staggered force platforms (model no. 2222 or OR6-5-1, Advanced Mechanical Technology Inc., Watertown, MA, USA) embedded in the walkway. The platforms measured ground reaction force and CP location at a precision of ~0.1 N and ~2 mm, respectively.

Human model
A human model was constructed in order to calculate physical quantities such as CM position and angular momentum. The model and coordinate system used in the study are shown in Fig. 1. The model comprises 16 rigid body segments: feet, tibias, femurs, hands, forearms, arms, pelvis-abdomen, chest, neck and head. The feet and hands were modeled as rectangular boxes. The tibia segments, femur segments, forearm segments and arm segments were modeled as truncated cones. The pelvis-abdomen and chest segments were modeled as elliptical slabs [ellipses in the horizontal (x–y) plane and extruded in the vertical (z) direction]. The neck was modeled as a cylinder, and the head was modeled as a sphere. The following 28 anthropometric measurements were taken for each study participant to accurately construct a representative model: (1) body weight, height, and total leg length measured from the medial malleolus to the anterior superior iliac spine; (2) lengths, widths and thicknesses of foot and hand segments; (3) segment lengths and proximal/distal base radii of tibia, femur, forearm and arm; (4) heights, widths and thicknesses of chest and pelvis-abdomen segments; and (5) radius of the head. The neck radius was set equal to half the head radius. The human model had a total of 38 degrees of freedom, or 32 internal degrees of freedom (12 for the legs, 14 for the arms, and six for the head, neck and trunk) and six external degrees of freedom.

For acceptance of the human model, we required that each segment's relative mass and density were in reasonable agreement with human morphological data from the literature (Winter, 1990). Relative mass was defined as segment mass divided by total body mass, and density as segment mass divided by segment volume. We accepted a segment design if both its relative mass and density fell within one standard deviation of the segment's mean experimental values from the literature. When the relative mass of each model segment was set equal to each segment's mean experimental value
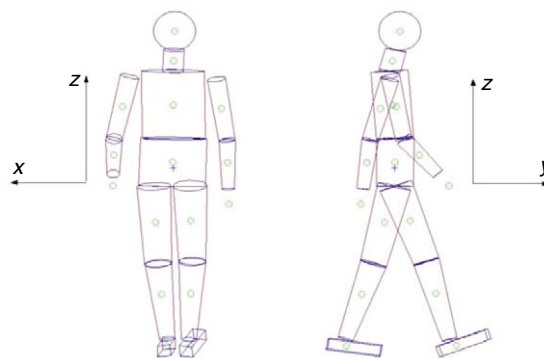

Fig. 1. Human model and coordinate frame. The human model has 16 segments with 32 internal degrees of freedom. Using human morphological data from the literature, mass is distributed throughout the model in a realistic manner. The coordinate frame is oriented by the right-hand rule with the z-axis directed vertically, the y-axis pointing in the direction of the walking motion (anterior–posterior direction), and the x-axis pointing to the right of the participant (medio-lateral direction).

from the literature, model segment density often became abnormal, falling beyond two standard deviations from the experimental mean. In distinction, when the density of each model segment was set equal to each segment's mean experimental value from the literature, model relative mass then became abnormal. As a resolution to this difficulty, we performed an optimization where model relative mass was varied until the error between model and experimental density values were minimized. We then confirmed that each segment's relative mass and density fell within one standard deviation of their experimental means reported in Winter (Winter, 1990).

In detail, the relative mass distribution throughout the model, M_R, described by a 16-component vector corresponding to the 16 segments of the model, was modeled as a function of a single parameter α such that:

$$M_R(\alpha) = (M_R^{Exp}+\alpha\vec{V}_R) / (1+\alpha) . \qquad (1)$$

Here M_R^{Exp} is a 16-component vector of mean relative mass values obtained from the literature (Winter, 1990), and $\vec{V}_R$ is a 16-component vector of relative volumes computed directly from the human model. The relative volume of the i-th segment, V_R^i, was defined as the ratio of the segment's volume, V^i, over the total body volume, V, or $V_R^i = V^i/V$. By using Eqn 1, total body mass and individual segment volumes computed from the model, model segment densities were computed and represented by a 16-component vector $\vec{D}(\alpha)$. Here the density of the i-th segment was defined as $D^i(\alpha) = M_{subject}M_R^i(\alpha)/V^i$, where $M_{subject}$ is total body mass and V^i is the volume of the i-th segment. The final relative mass distribution was obtained as $M_R = M_R(\alpha_{min})$ where α_{min} minimized the absolute error between the distribution of segment densities, $\vec{D}(\alpha)$, and the mean distribution of segment densities from the literature, $\vec{D}^{Exp}$. This analysis procedure may be expressed as:

$$\min|\vec{D}(\alpha) - \vec{D}^{Exp}| = \min\sqrt{\sum_i [D^i(\alpha) - D^{Exp,i}]^2}$$
$$\Rightarrow \alpha_{min} \Rightarrow \vec{M}_R = \frac{\vec{M}_R^{Exp} + \alpha_{min}\vec{V}_R}{1 + \alpha_{min}} . \quad (2)$$

Whole-body center of mass

The body's CM location was estimated using the human model and joint position data from the motion capture measurements. The CM position, $\vec{r}_{CM}$, of the entire 16-segment model was calculated as a sum of the products of the segments' relative masses and CM locations, or:

$$\vec{r}_{CM} = \sum_{i=1}^{16} M_R^i \vec{r}_{CM}^i . \qquad (3)$$

Here M_R^i is the relative mass of the i-th body segment, and $\vec{r}_{CM}^i$ is the CM location of the i-th body segment relative to the lab frame.

CM error estimate

To estimate the error in the CM calculation, we first collected kinematic data from the aerial phase of running and then, using Eqn 3, estimated the body's aerial phase CM trajectory. We found good agreement between this estimated CM trajectory and a ballistic trajectory ($R^2=0.99$; see Eqn 11 for R^2 definition). It was also noted that, during the aerial phase, the maximal distance error between these trajectories was less than 2 mm. As an additional check of CM error, we first collected kinetic and kinematic data while a participant stood on the force platform in a static standing pose.

The projection of the CM onto the horizontal ground surface, or x_{CM} and y_{CM} (see Fig. 1), was computed from the human model using Eqn 3, and then compared with the CP location measured directly from the force platform. The separation distance between the CM projection on the ground and the CP was ~3 mm. To determine whether the error changed appreciably for a different static pose, we repeated the experiment with one leg retracted rearward and the second leg protracted forward (comparable to the body's posture during the double-support phase of walking). Using this second pose, the CM model error was still small (~3 mm). At a self-selected gait speed, the body's CM oscillates with a peak-to-peak amplitude of between 4 and 5 cm in the medio-lateral (x) direction (Crowe et al., 1995). Thus, the estimated CM model error was less than 10% of these oscillations.

Whole-body angular momentum and moment

Whole-body angular momentum was estimated using the human model and kinematic gait data. Angular momentum, L, was calculated as the sum of individual segment angular momenta about the body's CM, or:

$$\vec{L} = \sum_{i=1}^{16} [(\vec{r}_{CM}^i - \vec{r}_{CM}) \times m_i(\vec{v}^i - \vec{v}_{CM}) + \vec{\tilde{I}}^i\vec{\omega}^i] . \qquad (4)$$

The first term within the square brackets is the angular momentum due to the i-th segment's CM movement. Here $\vec{r}_{CM}$ is the CM position of the entire body defined in Eqn 3, and $\vec{v}_{CM}$ is the whole-body CM velocity in the lab frame. Further, $\vec{r}_{CM}^i$ and $\vec{v}^i$ are the i-th segment's CM position and velocity in the lab frame, respectively, and m_i is the i-th segment's mass. The second term within the square brackets is the angular momentum of the i-th segment about its CM position. Here $\vec{\tilde{I}}^i$ and ^{i} are the i-th segment's inertia tensor (3×3) and angular velocity (3×1) about the segment's CM, respectively.

In order to reduce data variance across study participants, angular momentum was represented in dimensionless form using a normalization constant $N_{subject}$, equal to the product of the participant's mass $M_{subject}$, CM height $H_{subject}$, and the mean self-selected gait speed $V_{subject}$ across seven gait trials, or:

$$N_{subject} = M_{subject}V_{subject}H_{subject} . \qquad (5)$$

For each participant, the CM height was estimated during upright standing using the human model, the motion capture data, and Eqn 3. Angular momentum was computed using Eqn 4 for each gait cycle and then put into dimensionless form by dividing by the normalization constant $N_{subject}$ defined in Eqn 5. Dimensionless angular momentum was then plotted *versus* percentage gait cycle equal to gait time divided by total cycle time. At each percentage cycle time, the mean and standard deviation of the dimensionless angular momentum were computed over a total of 70 walking trials (10 participants, 7 gait trials per participant).

An alternative method for computing angular momentum is by integration of the moment about the CM. We computed angular momentum in this manner and compared the result to the angular momentum estimate of Eqn 4. We found little difference between these two estimates (R^2 values of 0.97, 0.96 and 0.98 for L_x, L_y and L_z, respectively). We preferred computing angular momentum directly from kinematics data because a single methodology could then be used when estimating both whole-body angular momentum and individual segment momenta in walking. The topic of individual segment angular momenta is addressed in the subsequent Materials and methods section entitled 'Segmental contributions to whole-body angular momentum'.

Angular momentum error estimate

To estimate the error in the angular momentum calculation, we first collected kinematic data from the aerial phase of running where angular momentum is a conserved quantity (assuming air drag exerts a negligible moment). From the flight phase kinematic data and Eqn 4, the angular momentum vector for the aerial phase was obtained, and one standard deviation about the mean value was assigned to be the model error for each spatial direction. To quantify its relative size, model error was then compared with the maximum angular momentum value found during the walking cycle about each spatial direction. Using walking data from the same study participant that participated in the running experiments, we first calculated the mean angular momentum curve for each spatial direction (n=7 walking trials). The maximum angular momentum values from the mean curves were then compared with the model errors for the three orthogonal directions. We found the angular momentum errors were 1.7%, 4.2% and 10% of the maximum angular momentum values in the medio-lateral (x), anterior–posterior (y) and vertical (z) directions, respectively (see Fig. 1 for coordinate frame specifications).

In addition to angular momentum, CM moment T was estimated by taking the rate of change of angular momentum at each percentage cycle time. Moment was then put into dimensionless form using the scaling factor $M_{subject}GH_{subject}$, where G is the gravitational constant. Similar to the angular momentum data analysis procedure, dimensionless CM moment was plotted *versus* percentage gait cycle, and at each percentage cycle time the mean and standard deviation were computed over a total of 70 walking trials.

Horizontal ground reaction force predictions

A key hypothesis in this paper is that angular momentum is highly regulated in steady-state human walking about all three orthogonal directions [$|L(t)|\approx 0$], and therefore horizontal ground reaction forces can be explained predominantly through an analysis that assumes zero net moment about the body's CM. To test this hypothesis, we first derived a relationship between horizontal ground reaction force, whole-body CM, and CP consistent with zero net moment. We then compared the predicted zero-moment forces with ground reaction forces measured directly from a force platform.

The horizontal component (hor) of the total moment about the CM [$T|_{hor}=(T_x,T_y)=(T_{CM}\cdot\vec{i},T_{CM}\cdot\vec{j})$] may be expressed as:

$$\vec{T}|_{hor} = [(\vec{r}_{CP}-\vec{r}_{CM}) \times \vec{F}]_{hor} = \frac{d\vec{L}}{dt}|_{hor} , \quad (6)$$

where $\vec{F}$ is the ground reaction force, and $\vec{r}_{CP}$ is the CP location on the ground surface. The CP ground reference point is frequently used in the study of human gait and postural balance (Winter, 1990; Rose and Gamble, 1994). For a body in contact with the force platform, the position of the CP, measured relative to a lab frame reference point located on the force platform walking surface, is calculated as:

$$x_{CP} = -\frac{M_y}{F_z} \quad (7)$$

and

$$y_{CP} = \frac{M_x}{F_z} , \quad (8)$$

where F_z is the measured vertical ground reaction force, and M_x and M_y are horizontal moments measured about that same lab reference point.

Eqn 6 can be solved for the horizontal ground reaction forces, or:

$$F_x = \underbrace{\left\{ \frac{F_z}{z_{CM}} (x_{CM}-x_{CP}) \right\}}_{F_x^{Zero\text{-}moment}} + \underbrace{\left\{ -\frac{T_y}{z_{CM}} \right\}}_{F_x^{Moment}} , \quad (9)$$

$$F_y = \underbrace{\left\{ \frac{F_z}{z_{CM}} (y_{CM}-y_{CP}) \right\}}_{F_y^{Zero\text{-}moment}} + \underbrace{\left\{ \frac{T_x}{z_{CM}} \right\}}_{F_y^{Moment}} , \quad (10)$$

where T_x and T_y are the CM moments in the medio-lateral (x) and anterior–posterior (y) directions, respectively. Throughout this manuscript we refer to the first and second terms on the right-hand sides of Eqns 9 and 10 as the zero-moment and moment force contributions[1] to the horizontal ground reaction forces, respectively (Popovic et al., 2005). To evaluate the hypothesis that horizontal ground reaction forces can be explained predominantly through a zero-moment analysis, zero-moment forces $F_x^{Zero\text{-}moment}$ and $F_y^{Zero\text{-}moment}$ were compared with the actual horizontal ground reaction forces measured from a force platform. As defined by Eqns 9 and 10, these zero-moment forces were obtained using the calculated position of body CM (Eqn 3), the experimentally measured CP, and the experimentally determined vertical ground reaction force.

To assess the amount of agreement between zero-moment model forces and experimentally measured horizontal forces, we used the coefficient of determination, R^2, where R^2=1 only if there is a perfect fit and R^2=0 indicates that the model's estimate is worse than using the mean experimental value as an estimate. More specifically, R^2 was defined as:

$$1 - \frac{\sum_{i=1}^{N_{Trial}} \sum_{j=1}^{N_{Percent}} (F_{Exp}^{ij}-F_{Mod}^{ij})^2}{\sum_{i=1}^{N_{Trial}} \sum_{j=1}^{N_{Percent}} (F_{Exp}^{ij}-\bar{F}_{Exp})^2} , \quad (11)$$

where F_{Exp}^{ij} and F_{Mod}^{ij} are the forces taken at the j-th percentage gait cycle of the i-th trial for the experimental data and model-predicted data, respectively. Before computing R^2 values for each spatial direction and study participant, both experimental and zero-moment forces for the medio-lateral (x) and anterior–posterior (y) directions were plotted *versus* percentage gait cycle (equal to gait time divided by total cycle time). We then computed medio-lateral (x) and anterior–posterior (y) R^2 values for each participant by summing over all walking trials (N_{Trial}=7) and gait percentage times analyzed ($N_{Percent}$=100).

In Eqn 11, experimental mean $\bar{F}_{Exp}$ is the grand mean over all walking trials and gait percentage times analyzed, or:

$$\bar{F}_{Exp} = \frac{1}{N_{Trial}N_{Percent}} \sum_{i=1}^{N_{Trial}} \sum_{j=1}^{N_{Percent}} F_{Exp}^{ij} . \quad (12)$$

[1]It is noted that moment as used here refers to horizontal moment and not vertical moment.

We used a non-parametric Wilcoxon matched-pairs test (Wilcoxon, 1945) for comparing the two R^2 values corresponding to the medio-lateral (x) and anterior–posterior (y) directions. This statistical significance test was performed to look for differences in the capacity of the zero-moment force model to predict experimental force equally well in the two horizontal directions.

Center of pressure predictions

An alternative strategy for quantifying the degree to which whole-body angular momentum is regulated in walking is to estimate a zero-moment CP position. This ground reference point, previously defined in the robotics literature, is called the centroidal moment pivot (CMP) (Herr et al., 2003; Hofmann, 2003; Popovic et al., 2004a; Popovic et al., 2005; Goswami and Kallem, 2004). The CMP location, $\vec{r}_{CMP}$, is defined as the point where a line parallel to the ground reaction force, passing through the CM, intersects with the ground surface. As its name implies, when the CMP coincides with the CP, no horizontal moments act about the body's CM. In distinction, when these ground reference points diverge, non-zero horizontal CM moments exist. To further quantify whole-body rotational dynamics, we compare a calculated CMP trajectory with an experimentally measured CP trajectory from the force platforms.

The CMP can be expressed mathematically by requiring that the cross-product of the CMP–CM position vector and the ground reaction force vector vanishes, or:

$$[(\vec{r}_{CMP} - \vec{r}_{CM}) \times \vec{F}]_{hor} = 0 . \tag{13}$$

By expanding this cross-product, the CMP location can be written in terms of the CM location and the ground reaction force, or:

$$x_{CMP} = x_{CM} - \frac{F_x}{F_z} z_{CM} \tag{14}$$

and

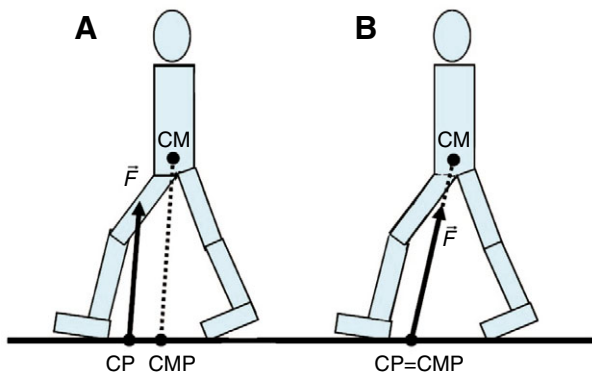$$y_{CMP} = y_{CM} - \frac{F_y}{F_z} z_{CM} . \tag{15}$$

Fig. 2. Centroidal moment pivot (CMP). The CMP is the point where the ground reaction force would have to act to keep the horizontal component of the whole-body angular momentum constant. When the moment about the center of mass (CM) is zero (B), the CMP coincides with the center of pressure (CP). However, when the CM moment is non-zero (A), the extent of separation between the CMP and CP is equal to the magnitude of the horizontal component of moment about the CM, divided by the normal component of the ground reaction force.

When the CMP departs from the CP, there exist non-zero horizontal CM moments, causing variations in whole-body angular momentum (see Fig. 2A). While by definition the CP cannot leave the ground support base[2], the CMP can – but only when horizontal moments act about the CM. In this investigation, the CMP was calculated using Eqn 14 and 15, the calculated CM position from the human model, and the ground reaction force measured from the force platforms. We then computed the mean separation distance between the CMP and CP points, normalized by foot length, across the entire gait cycle. If angular momentum is highly regulated in walking and CM moments are small, we anticipate that the CMP location should coincide with the experimentally measured CP position (see Fig. 2B).

Segmental contributions to whole-body angular momentum

Motivated by Elftman (Elftman, 1939), in this paper we tested the hypothesis that whole-body angular momentum is small throughout the walking cycle, despite substantial segmental momenta, indicating large segment-to-segment cancellations. To investigate the segmental movement correlations in connection with angular momentum, we used principal component (PC) analysis. We first obtained the segmental angular momentum PCs together with the amount of data explained by each PC. We then calculated their respective weighting coefficients, or tuning coefficients. Finally, we obtained the level of momentum cancellation between body segments for all three spatial directions, and the strategy employed by the body to achieve that level of cancellation.

Principal component analysis

PC analysis (e.g. Jackson, 1991) was performed on all segmental angular momenta, for each of the three spatial components, to produce PCs. Each PC was a 16-component unit vector, P_j^i, corresponding to the 16 body segments of the human model. Here P_j^i represents the i-th PC in the j-th direction. Vector components P_j^{iq} denoted the relative contributions of the q-th body segment to P_j^i. As is customary, each PC was assigned a value for the percentage of data explained, DE^i_j, where $j=1...3$ denotes the number of spatial components, and $i=1...N$ corresponds to the total number of PCs (equal to the number of human model segments, i.e. $N=16$).

The PC vectors and the corresponding percentages of data explained were obtained using the MATLAB statistical toolbox (MathsWorks Inc., Natick, MA, USA). The 16-component angular momentum vector was compactly represented as:

$$\vec{\Lambda}_j(t) = \sum_{i=1}^{N} C_j^i(t) \cdot \vec{P}_j^i, \tag{16}$$

where $C_j^i(t)$, $t \in (0\%, 100\%)$ are time-dependent tuning coefficients. The components of the momentum vector defined in Eqn 16 correspond to the 16 segments of the human model.

Normalized tuning coefficients

In order to extract directional dependence, we introduced the normalized tuning coefficients $c_j^i(t)$, such that:

$$\vec{\Lambda}_j(t) = \left\{ \sqrt{\sum_{i=1}^{N} [C_j^i(t)]^2} \right\} \sum_{i=1}^{N} c_j^i(t) \cdot \vec{P}_j^i, \tag{17}$$

[2]When in single support, the support base is the outline of the part of the stance foot that is actually in contact with the ground. When in double support, where both feet are on the ground, the support base is the smallest convex shape that includes all points where both feet are in contact with the ground.

where the expression in the brackets represents the magnitude of the angular momentum vector in the N-dimensional space. It is noted here that the time-dependent normalized tuning coefficients satisfy:

$$\sum_{i=1}^{N} |c_j^i(t)|^2 = 1 , \quad \forall \, j = 1...3 , \quad t \in (0\%, 100\%) . \quad (18)$$

Analysis was performed to find the smallest number of angular momentum PCs necessary to explain greater than 90% of the segmental angular momentum data. To determine the minimum number of PCs to capture both inter- and intrasubject variability, both participant-dependent and participant-independent analysis methods were performed. For the participant-dependent method, PC analysis was performed for each participant across seven walking trials, whereas for the participant-independent method, PC analysis was conducted across all participants and walking trials (70 trials).

Segmental angular momentum cancellation
The participant-dependent PCs were used to estimate the amount of segmental momentum cancellation for each participant and j-th spatial direction, or:

$$S_j = 1 - \sqrt{ \sum_{i=1}^{N_E} DE_j^i \left[\frac{\sum_{q=1}^{16} P_j^{iq}}{\sum_{q=1}^{16} |P_j^{iq}|} \right]^2 } , \quad (19)$$

where $q=1...N$ and where $N_E=4$ sufficed for the level of precision in our study. The net cancellation was therefore expressed as a sum of squares (i.e. treated as independent variables or orthogonal directions) of cancellations, across the largest PCs, weighted by their respective data explained.

To test whether the amount of angular momentum cancellation for all 10 participants across the three spatial directions was sampled from the same distribution, we used a non-parametric Friedman ANOVA test (Friedman, 1937; Friedman, 1940). This statistical significance test was performed to look for differences in the amount of angular momentum cancellation across the three orthogonal directions, or vertical (z), anterior–posterior (y) and medio-lateral (x). Two types of non-parametric *post hoc* tests were independently performed to compare cancellation for pairs of spatial directions. These tests were the Dunn procedure with Wilcoxon test (Wilcoxon, 1945; Dunn, 1964) and the minimum significant difference (Portney and Watkins, 2000).

RESULTS
Whole-body angular momentum and moment
Angular momentum estimations
To quantify whole-body rotational behavior during steady-state walking, angular momentum was computed from kinematic gait data, as defined in Eqn 4. Angular momentum curves, scaled by $M_{subject}V_{subject}H_{subject}$, are shown in Fig. 3A *versus* percentage gait cycle. Throughout the gait cycle, the absolute value of the normalized angular momentum mean, plus one standard deviation, remains smaller than 0.05, 0.03 and 0.01 in the medio-lateral (x), anterior–posterior (y) and vertical (z) directions, respectively[3].

[3]The angular momentum curves shown in Fig. 3A agree well with the measurements of Elftman (Elftman, 1939), in terms of overall curve shape, as well as peak momentum values in the medio-lateral (x), anterior–posterior (y) and vertical (z) directions.

To provide the reader with a better understanding of the relative size of these measured human values, we computed the angular momentum about the CM of single-segment, rigid-body models. In the vertical (z) direction, we computed the angular momentum about the CM of a rigid body rotating about a stationary vertical axis passing through the stance foot with an angular velocity equal to $V_{subject}/W$, where W is half the foot separation distance in the medio-lateral (x) direction during quiet standing. The angular momentum, scaled by $M_{subject}V_{subject}H_{subject}$, for this simple comparison case is then equal to $I_{zz}/(M_{subject}H_{subject}W)$. Using the human model and kinematic data from the 10 study participants, we computed the average I_{zz} value during the single-support phase for all 10 participants. Using this value, the normalized angular momentum for the rotating rigid body was equal to ~0.05, 5-fold larger than our measured human angular momentum value of 0.01 in the vertical (z) direction.

In the medio-lateral (x) direction, the normalized angular momentum about the CM of a physical inverted pendulum falling forward while rotating about a stationary rotational axis at the ground surface is $I_{xx}/(M_{subject}H_{subject}^2)$, assuming an angular velocity equal to $V_{subject}/H_{subject}$ and a moment of inertia about the CM equal to I_{xx}. Once again, using the human model and kinematic data from the 10 study participants, we computed the average I_{xx} value during the single-support phase for all 10 participants. Using this value, the normalized angular momentum for the physical inverted pendulum falling forward was equal to ~0.2, 4-fold larger than our measured human angular momentum value of 0.05 in the medio-lateral (x) direction.

The authors cannot think of a simple comparison case for the peak angular momentum in the anterior–posterior (y) direction. Thus, the normalized peak human value of 0.03 in the anterior–posterior (y) direction can be compared with both the medio-lateral (x) and the vertical (z) single-segment, rigid-body values; the vertical (z) rigid body value of 0.05 is 1.7-fold larger, and the medio-lateral (x) value of 0.2 is over 6-fold larger, than the human value of 0.03.

CM moment estimations
Moment curves, scaled by $M_{subject}GH_{subject}$, are shown in Fig. 3B *versus* percentage gait cycle. Throughout the gait cycle, the absolute value of the normalized CM moment mean, plus one standard deviation, remains smaller than 0.07, 0.03 and 0.014 dimensionless units in the medio-lateral (x), anterior–posterior (y) and vertical (z) directions, respectively.

Horizontal ground reaction force and CP predictions
In Fig. 4A,B, zero-moment and experimental forces are plotted *versus* percentage gait cycle for the medio-lateral (x) and anterior–posterior (y) directions, respectively. Plotted data are for one representative participant (participant no. 1 in Table 1) and experimental trial. Mean R^2 values for each participant, and across all participants, are listed in Table 1. Across all study participants, the mean R^2 value is 0.91±0.06 in the medio-lateral (x) direction and 0.90±0.03 in the anterior–posterior (y) direction. The high R^2 values indicate good agreement between zero-moment force predictions and experimental force values. No significant difference was observed between the distributions of R^2 values for these two spatial directions ($P=0.267$), indicating that the zero-moment model has an equal capacity to predict horizontal ground reaction forces independent of horizontal direction.

Additionally we calculated the CMP using Eqn 14 and 15, and then compared the values with the experimentally measured CP
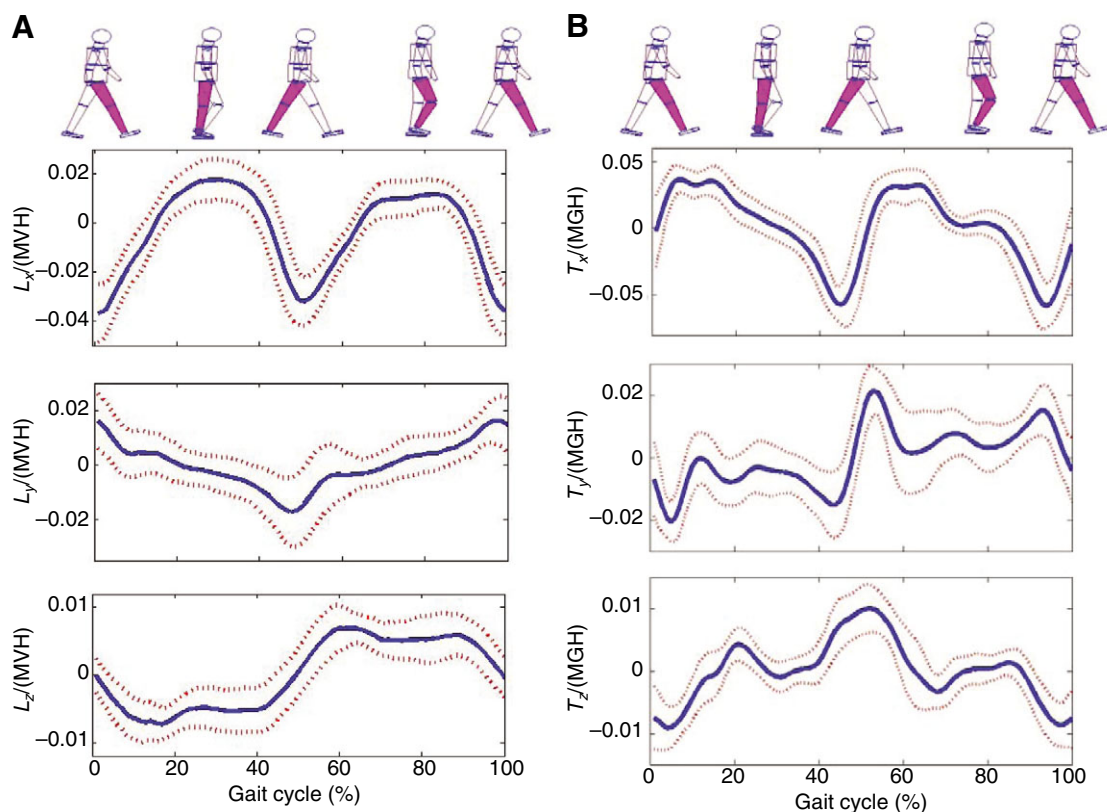
Fig. 3. Whole-body angular momentum and moment. (A) A normalized angular momentum for walking is plotted about three orthogonal directions *versus* percentage gait cycle. The angular momentum is normalized by the product of each participant's mass, CM height and self-selected gait speed (*MVH*; see Table 1 for values). (B) Normalized CM moment is plotted about three orthogonal directions *versus* percentage gait cycle. Moment is normalized by the product of each participant's weight and CM height (*MGH*). For both A and B, the solid line is the mean normalized value, and the dashed lines are one standard deviation about the mean (10 participants and seven walking trials per participant). In addition, 0% and 100% gait cycles correspond to consecutive heel strikes of the same foot.

from a force platform. In Fig. 4C, the CP, CMP and CM ground projection locations are plotted. Again, plotted data are for one representative participant (participant no. 1 in Table 1) and experimental trial. Table 1 includes the mean distance between the

Table 1. Body mass $M_{subject}$, CM height $H_{subject}$ and self-selected walking speed $V_{subject}$ for each study participant

Participant	$M_{subject}$ (kg)	$H_{subject}$ (m)	$V_{subject}$ (m s^{-1})	R_x^2	R_y^2	β%
1	50.1	0.88	1.30	0.97	0.94	16
2	62.7	0.94	1.38	0.97	0.90	13
3	81.9	1.08	1.32	0.96	0.92	12
4	73.9	1.01	1.18	0.95	0.85	16
5	49.9	0.88	1.06	0.95	0.90	15
6	57.2	0.92	1.40	0.95	0.87	10
7	82.6	1.08	1.24	0.91	0.88	12
8	64.6	1.03	1.41	0.82	0.84	12
9	65.3	0.99	1.40	0.83	0.95	15
10	76.8	1.06	1.33	0.81	0.91	15
Mean ± s.d.	66±12	1.0±0.1	1.3±0.1	0.91±0.06	0.90±0.03	14±2

Also listed are the mean coefficients of determination R^2 between the zero-moment force curve and the experimentally measured horizontal ground reaction force for medio-lateral (R_x^2) and anterior-posterior (R_y^2) directions (see Eqn 11), and the mean distance between the CMP and CP points across the entire gait cycle normalized by foot length for each study participant (β%) is given.

CMP and CP points, normalized by foot length, across the entire gait cycle, or β%. The mean normalized distance across participants is small (β=14±2%), indicating good agreement between the CMP and CP points in steady-state walking. Finally, for all participants and walking trials, the CMP remains within the ground support base throughout the walking cycle, indicating how closely the human body regulates angular momentum in walking.

Segmental contributions to whole-body angular momentum
For the participant-dependent analysis approach, the data explained by the first PC, as well as the first three PCs combined, are shown in Table 2. On average across all study participants, the first three PCs accounted for 98±1%, 92±2% and 95±1% in the medio-lateral (*x*), anterior–posterior (*y*) and vertical (*z*) directions, respectively. Thus, the participant-dependent PC analysis performed on each participant's trial data reveals that only three PCs are necessary to explain greater than 90% of segmental momentum data. In Fig. 5, the average participant-dependent first PC is shown for all three spatial directions. Standard deviation error bars are included to quantify the level of variability in the first PC across study participants. The greatest variability in the segmental momentum distribution was found to occur in the coronal plane (*x–z* plane in Fig. 1).

The results of participant-independent PC analysis performed simultaneously on all participants and trials (total of 70 trials) are shown in Figs 6 and 7. In Fig. 6, the angular momentum PCs, that
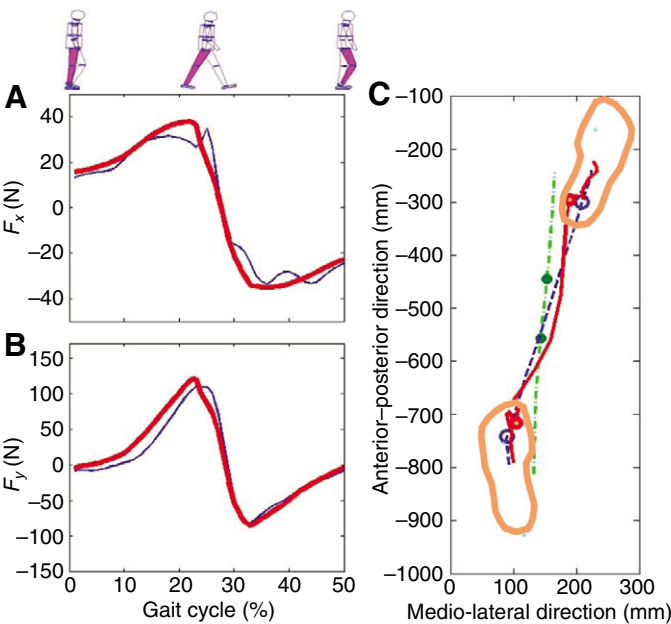
Fig. 4. Horizontal ground reaction force and CP predictions. (A,B) The horizontal ground reaction forces in walking are plotted *versus* percentage gait cycle in the medio-lateral (*x*) and anterior–posterior (*y*) directions, respectively. The thick red line is the calculated zero-moment force (see Eqns 9 and 10), and the thin blue line is the force measured experimentally using force platforms. (C) Plotted are the CP (blue dashed line), CMP (red solid line) and CM ground projection (green dash-dotted line) trajectories and corresponding footprints. The two circles on each line denote the transition from single to double support, and *vice versa*. In all plots, only half the gait cycle is shown. Data span from the middle of a single-support phase (0% gait cycle) to the middle of the next single-support phase of the opposite limb (50% gait cycle). Data shown are for one representative participant and trial (participant no. 1 in Table 1).

found that whole-body angular momentum is small, despite substantial segmental momenta, indicating large segment-to-segment cancellations: 95% medio-lateral (*x*) cancellation, 69% anterior–posterior (*y*) cancellation and 77% vertical (*z*) cancellation. We found no significant difference between the amount of momentum cancellation in the anterior–posterior (*y*) and vertical (*z*) directions ($P=0.19$). However, we did find a significant difference between the amount of momentum cancellation in the medio-lateral (*x*) direction compared with the anterior–posterior (*y*) direction ($P=0.001$) and the vertical (*z*) direction ($P=0.002$).

In Fig. 7, the mean normalized tuning coefficients, as defined in Eqn 17, are shown for three spatial directions. The tuning coefficients correspond to the PCs plotted in Fig. 6, and define the relative dominance of each PC as a function of gait cycle. In the subsequent sections, we use the PCs, and their respective tuning coefficients, to describe segment-to-segment momentum cancellations.

Segmental cancellation in the medio-lateral direction

The most dominant first PC in the medio-lateral (*x*) direction shows that adjacent leg-segment momenta oppose one another (the left foot momentum cancels the right foot momentum, etc.; see Fig. 6). Further, the first PC shows that arm, abdomen, pelvis, chest, neck and head momenta are negligible. However, as the first tuning coefficient in the medio-lateral (*x*) direction shows in Fig. 7, the first PC becomes less dominant during the powered plantar flexion phase, from 43% to 62% gait cycle, and the second PC increases in dominance.

For the second PC, cancellation occurs within each leg, in contrast to the first PC where cancellation occurs from leg segment to adjacent leg segment. For the trailing limb, foot and calf momenta oppose thigh momentum during ankle-powered plantar flexion, pre-swing knee flexion, and pre-swing hip flexion. For the forward limb, foot and calf momenta oppose thigh momentum during ankle-controlled plantar flexion, early stance knee flexion and early stance hip flexion.

Segmental cancellation in the anterior–posterior direction

The most dominant first PC in the anterior–posterior (*y*) direction shows that foot, calf, chest and head momenta oppose the abdomen and pelvis momenta, and further that arm, thigh and neck momenta are negligible (see Fig. 6). However, as the first tuning coefficient in the anterior–posterior (*y*) direction shows, the first PC is most dominant during the double-support phase of walking, from 0% to 12% gait cycle and from 50% to 62% gait cycle. During single support, the first PC is not as dominant, and the second, third and fourth PCs increase in dominance. It is noted here that for the second PC, explaining 29% of the data, no dominant segmental cancellation occurs.

Segmental cancellation in the vertical direction

The first PC in the vertical (*z*) direction shows that leg angular momenta oppose the remaining body segment momenta of the arms, pelvis, abdomen, chest, neck and head. However, the first PC becomes less dominant during the powered plantar flexion phase, from 43% to 62% gait cycle, and the second and third PCs increase in dominance (see Fig. 7). However, the

when combined account for more than 90% of the experimental data, are shown for three spatial directions. While only three PCs are needed to explain more than 90% of the data in sagittal (*y*–*z*) and transverse (*x*–*y*) planes, four PCs are needed in the coronal (*x*–*z*) plane.

The percentage of segmental momentum cancellation (see Eqn 19) per participant and spatial direction is listed in Table 2. We

Table 2. The data explained (*DE*) by the first principal component (PC), as well as the first three PCs combined, listed for each participant and spatial direction

Participant	DE_x^1	DE_y^1	DE_z^1	DE_x^{III}	DE_y^{III}	DE_z^{III}	S_x	S_y	S_z
1	87	73	86	99	93	94	96	92	73
2	89	75	82	98	92	94	96	92	74
3	86	49	85	98	91	95	93	64	63
4	86	66	89	99	94	95	93	52	80
5	87	67	89	99	90	95	93	89	81
6	90	65	90	99	94	95	97	74	79
7	86	57	87	98	93	95	95	71	79
8	83	78	85	97	92	93	93	84	94
9	88	65	89	99	90	97	96	44	69
10	87	85	88	98	95	97	95	21	78
Mean ± s.d.	87±2	68±10	87±2	98±1	92±2	95±1	95±2	69±23	77±8

DE_x^1 (%) denotes the percentage of data explained by the first PC in the *x*-direction, and DE_x^{III} (%) denotes the data explained by the first three PCs combined in the *x*-direction. Also listed is the percentage of angular momentum cancellation, *S* (%) defined in Eqn 19, for each participant and spatial direction.
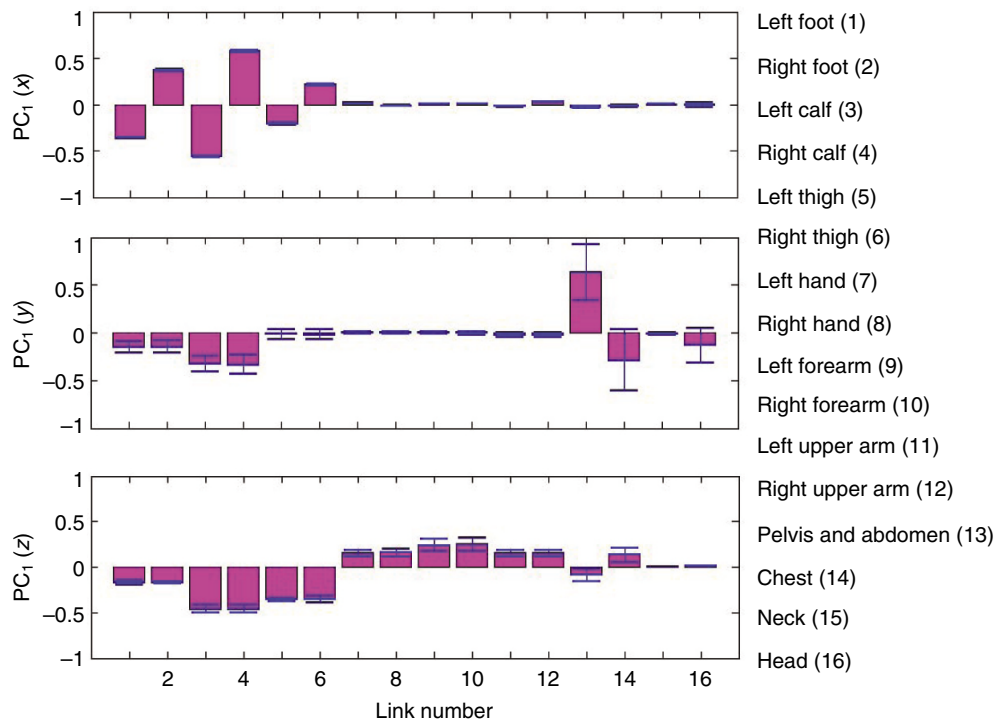
Fig. 5. The mean participant-dependent first PC about three spatial directions. Here the participant-dependent first PCs were averaged across the 10 study participants. Error bars are one standard deviation about the mean. The abscissa numbers and human model segments are paired to the right of the figure. In the anterior–posterior (y) direction, large variations in the relative contribution of angular momentum are observed for the pelvis and abdomen (segment 13), chest (segment 14) and head (segment 16) [see large standard deviations in Fig. 5 for PC_1 (y)].

second and third PCs only explain ~4% of the data, and thus the rotational dynamics that they explain are not discussed here.

DISCUSSION
Would simple inverted pendulum mechanics also predict the observed horizontal ground reaction forces?
The inverted pendulum model has been used by researchers to describe sagittal-plane CM dynamics during the single support phase of walking (Bekker, 1956; Cavagna et al., 1976; Alexander, 1976; Margaria, 1976; Cavagna et al., 1977). The model comprises a point mass attached to a mass-less rigid leg that intersects with the ground surface at a single point. The model makes three critical assumptions. First, that the body moves as if all its mass is located at the CM, requiring that the resultant ground reaction force vector always points at the CM (zero-moment condition). Second, that the CP is a stationary, time-invariant point. And finally, that the leg during single support behaves as a rigid strut.

This study directly addresses the first two assumptions of the inverted pendulum model. Since the entire mass of the body is represented as a point mass, the model will, by definition, always move with a constant angular momentum and with no moments acting about its CM. The data presented in this study support the point mass representation, assumed by many recent walking models (Kuo, 2002; Geyer et al., 2006; Srinivasan and Ruina, 2006). In fact, we further generalize the point mass representation to include single- and double-support phases. We found that zero-moment forces agree remarkably well with experimental values for single support ($R_x^2=0.97\pm0.02$; $R_y^2=0.94\pm0.02$), and agree reasonably well for double support ($R_x^2=0.72\pm0.14$; $R_y^2=0.78\pm0.06$). Still further, whereas the inverted pendulum model is a 2-D sagittal plane model, the results of this study further generalize the point mass representation to include the medio-lateral (x) direction. Across all study participants and including the entire gait cycle, the mean R^2 parameter was 0.91 ± 0.06 in the medio-lateral (x) direction and 0.90 ± 0.03 in the anterior–posterior (y) direction. No significant difference was observed between the distributions of R^2 values for

these two spatial directions ($P=0.267$), indicating that zero-moment forces are equally dominant in the two horizontal directions.

Not all assumptions of the inverted pendulum model are supported by this investigation. The fact that the model assumes that the CP acts as a fixed point limits its capacity to predict horizontal ground reaction force and CM dynamics. For the zero-moment force predictions shown in Fig. 4A,B, the CP was not represented as a fixed point, but rather experimental CP trajectories were used as inputs, as dictated by Eqns 9 and 10. As noted earlier, zero-moment forces closely match horizontal ground reaction forces during single support ($R_x^2=0.97\pm0.02$; $R_y^2=0.94\pm0.02$). In contrast, using a fixed CP point as required by the inverted pendulum model[4], the calculated horizontal forces agree well in the medio-lateral (x) direction ($R_x^2=0.88\pm0.08$) but the agreement is very poor in the anterior–posterior (y) direction ($R_y^2=-0.33\pm0.44$). Not surprisingly, for double support a fixed CP analysis results in extremely poor agreement between zero-moment and experimental forces ($R_x^2=-0.28\pm0.22$; $R_y^2=-0.11\pm0.53$). In summary, for the advancement of bipedal walking models that accurately predict steady-state CM dynamics, we feel a point mass representation can be assumed, but the mechanical behavior of the model's legs and their interaction with the ground surface must be sufficiently human-like so as to achieve realistic CP dynamics.

Is angular momentum always regulated during human movement tasks?
Whole-body angular momentum regulation is not a general feature across all human movement tasks. For some movement patterns, humans purposefully generate angular momentum to enhance stability and maneuverability (Popovic et al., 2004b; Hofmann et al., 2007). By actively rotating body segments (arms, torso, legs), CM moments can be generated that cause horizontal moment forces

[4]For the stationary CP analysis, the zero-moment force components of Eqns 9 and 10 were used where the CP position was assumed to be at a fixed, lab frame location, corresponding to a point at the foot center for single support and halfway between both feet for double support.
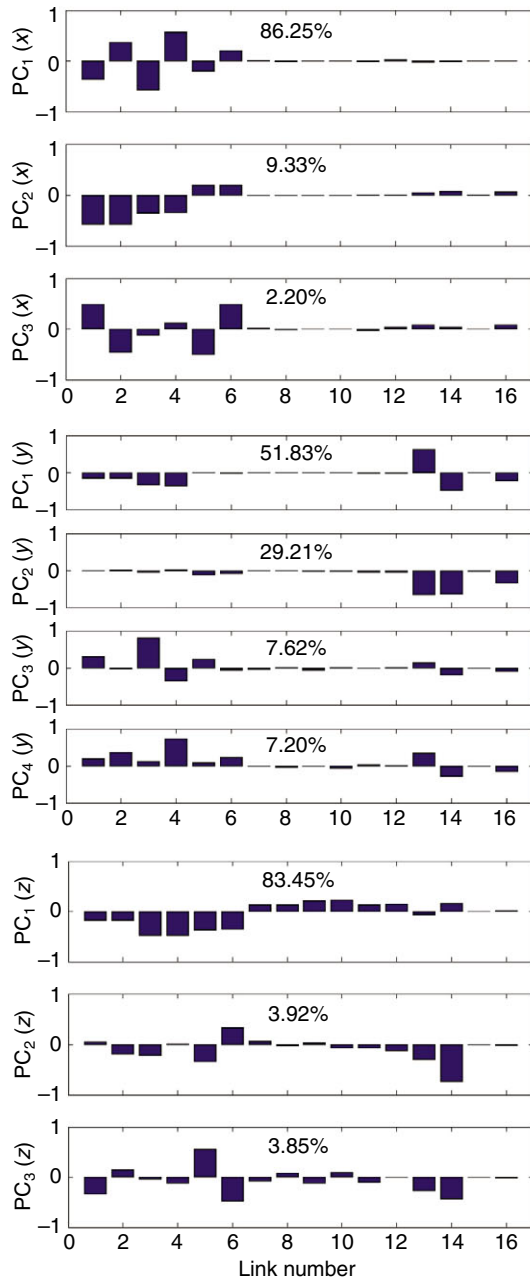
Fig. 6. The participant-independent PCs about three spatial directions. Plotted are the PCs that when combined account for more than 90% of experimental data. The abscissa numbers correspond to the same human model segments as defined in Fig. 5. While only three PCs are needed to explain 90% of the data in the sagittal and transverse planes, four PCs are required in the coronal (*x*–*z*) plane.
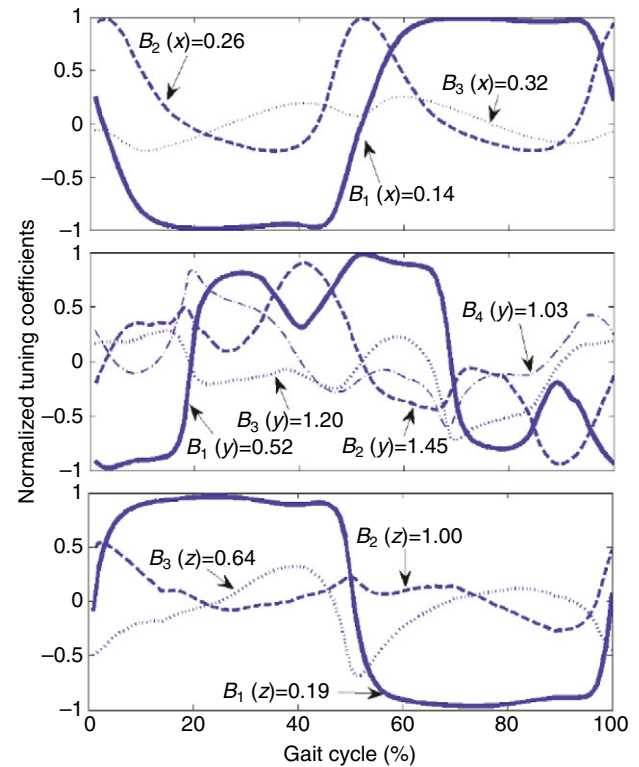

Fig. 7. Tuning coefficients. The mean values, over all participants and trials, of the normalized tuning coefficients are plotted for three spatial directions. The tuning coefficients correspond to the PCs shown in Fig. 6. Here the normalized tuning coefficients were computed using Eqn 17, and were obtained as gait percentage averages over all participants and walking trials. To provide information on the variability of each normalized tuning coefficient, a variability number $B_i(j)$ is assigned to each curve, where $j=1...3$ (spatial directions) and $i=1...N$ (model segments or PCs). Each number was computed by first estimating the area between plus and minus one standard deviation about the tuning coefficient mean, and then dividing by the total area beneath the tuning coefficient mean – from 0% to 100% gait cycle.

to act on the CM, as defined by Eqns 9 and 10. This strategy allows humans to perform movement tasks that would not otherwise be possible. For example, while balancing on one leg, humans are capable of repositioning the CM just above the stance foot from an initial body state where CM velocity is zero, and the ground CM projection is outside the foot support envelope[5] (Hofmann et al.,

2007). Such a stability feature cannot be achieved using a bipedal control scheme that simply applies a zero-moment, constant angular momentum control. Clearly, if the ground CM projection falls outside the support envelope and the CM velocity is zero, the zero-moment force does not act to restore CM position, but rather continually accelerates the CM away from the stance foot. This fact can be easily verified by reviewing the zero-moment force component from Eqn 9, or $F_x^{\text{Zero–moment}}=F_z(x_{\text{CM}}-x_{\text{CP}})/z_{\text{CM}}$. Imagine the case where a person is trying to balance on his right leg, and a laterally directed force disturbance causes x_{CM} to move beyond the foot envelope in a lateral, positive direction (positive *x*-direction as defined in Fig. 1). Since x_{CP} cannot extend beyond the foot's lateral edge, $x_{\text{CM}}-x_{\text{CP}}$ is positive, making the CM zero-moment force positive, and causing the CM to move farther from the stance foot. The only way a person can successfully balance on one leg from these initial conditions is to actively generate angular momentum. By rotating arms, trunk, head and swing leg, a CM moment in the positive *y*-direction can be generated, causing a negative moment force, $F_x^{\text{Moment}}=-T_y/z_{\text{CM}}$, that can restore the CM back to a position directly over the stance foot (Hofmann et al., 2007). This behavior can be observed in tightrope walking. Here body segments are accelerated to generate angular momentum about the CM and to
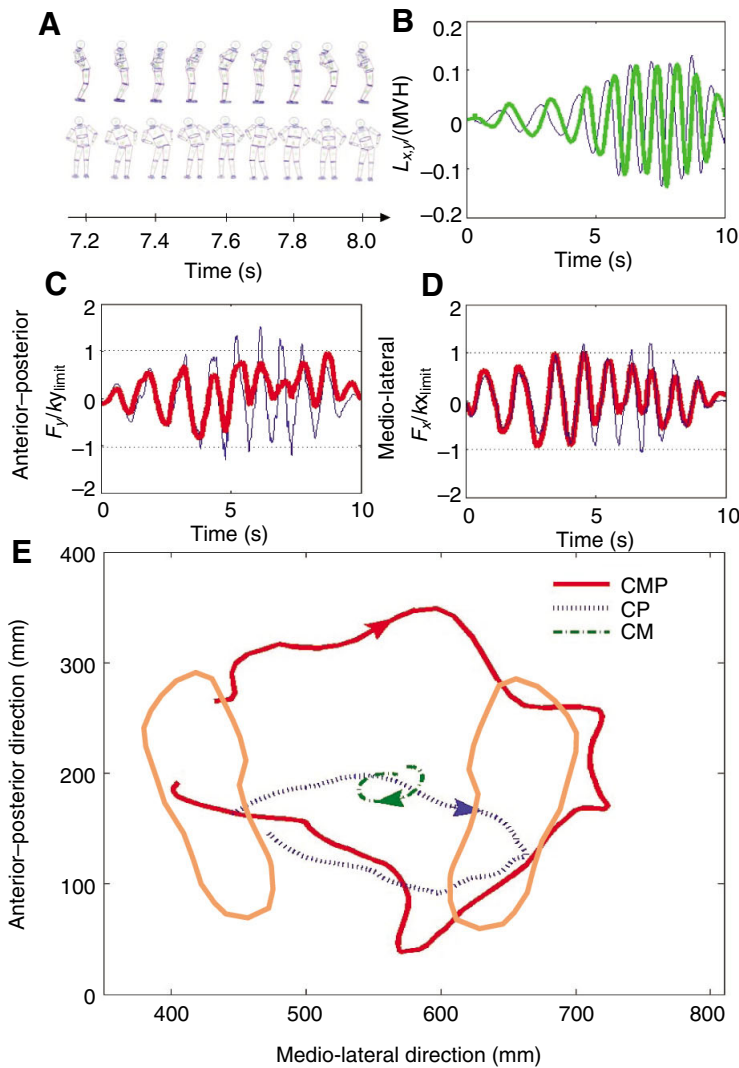
Fig. 8. Hula-hoop body motions. Angular momentum, horizontal ground reaction force and ground references points are plotted in the medio-lateral (x) and anterior–posterior (y) directions. In this experiment a participant rotated his hips while standing in double support, similar to how one twirls a hula hoop, at an increasing and then decreasing rotational speed for approximately 10 s (see A for one representative cycle). (B) The horizontal components of normalized angular momentum are plotted *versus* time. For ease of comparison with walking values shown in Fig. 3A, the angular momentum is normalized by the product of the participant's mass, CM height and self-selected gait speed (*MVH*; see participant no. 1 in Table 1). (C,D) The horizontal ground reaction forces measured experimentally (thin blue line) are plotted along with the calculated zero-moment forces (thick red line) *versus* time for the same participant and trial as in B. Both experimental and calculated zero-moment forces are normalized by the stiffness term, F_z/z_{CM}, and the radius of the ground support base in the appropriate direction (see Eqns 9 and 10). In the medio-lateral (x) direction, the radius was measured while standing in double support, and was equal to one-half the distance from the lateral edge of the right foot to the lateral edge of the left foot. In the anterior–posterior (y) direction, the radius was equal to one-half the participant's foot length. (E) Plotted are the CP (blue dashed line), CMP (red solid line) and CM ground projection (green dash-dotted line) trajectories and corresponding footprints. As in A, only one hula-hoop cycle is shown from 7.2 to 8 s. The ground CM projection remains within the support envelope while the CMP often falls outside the region.

create a moment force that restores the CM position over the stance foot.

To further investigate movement tasks where the moment force is dominant, we conducted two pilot investigations. We first analyzed a particular movement task while standing in double support. Here a study participant rotated his hips, similar to how one twirls a hula-hoop, at an increasing and then decreasing speed for approximately 10 s (see Fig. 8A). Kinetic and kinematic data were collected using the same experimental setup employed in the walking study, and the same human model was then used for physical modeling.

In Fig. 8B, the horizontal components of normalized angular momentum are plotted *versus* time, showing angular momentum values that are approximately an order of magnitude larger than the steady-state walking values shown in Fig. 3A. Further, in Fig. 8C,D, we show zero-moment forces, as well as experimental forces measured from a force platform, for the hula-hoop twirling motion. Here the difference between the two curves is equal to the moment force component of the horizontal ground reaction forces, as defined by Eqns 9 and 10. Beyond $t=5$ s, there is no longer good agreement between zero-moment forces and experimental values as CM moment, or the rate of change of angular momentum, becomes dominant. During this same time period, as is shown in

Fig. 8E, the CMP ground reference point often moves beyond the ground support envelope, diverging from the CP and the ground CM projection. This dynamical behavior is distinct from that of steady-state normal walking where the CMP never leaves the ground support base, as indicated in Fig. 4C.

For the hula-hoop motion, angular momentum becomes sufficiently large that moment forces become dominant over zero-moment forces, and the CMP moves beyond the support envelope. Between $t=6$ s and $t=8$ s in Fig. 8C,D, the moment force is often as large as, or larger than, the zero-moment force. Even with the existence of large CM moments, the participant still remains upright and stable. The regulation of angular momentum [$|L(t)|{\approx}0$] is therefore not a necessary condition for human stability. This finding is in direct disagreement with the arguments of Morasso and Schieppati (Morasso and Schieppati, 1999) and Morasso et al. (Morasso et al., 1999), who stated that the 'CP–CM phase-lock', a relation similar to the zero-moment force component of Eqns 9 and 10, is a pure physics consequence of stability. In fact, the generation of angular momentum and CM moments is a key strategy for the enhancement of bipedal maneuverability and stability (Popovic et al., 2004b; Hofmann et al., 2007). Clearly, the CM motions found in the hula-hoop task could not be achieved using only a constant angular moment, zero-moment control approach.
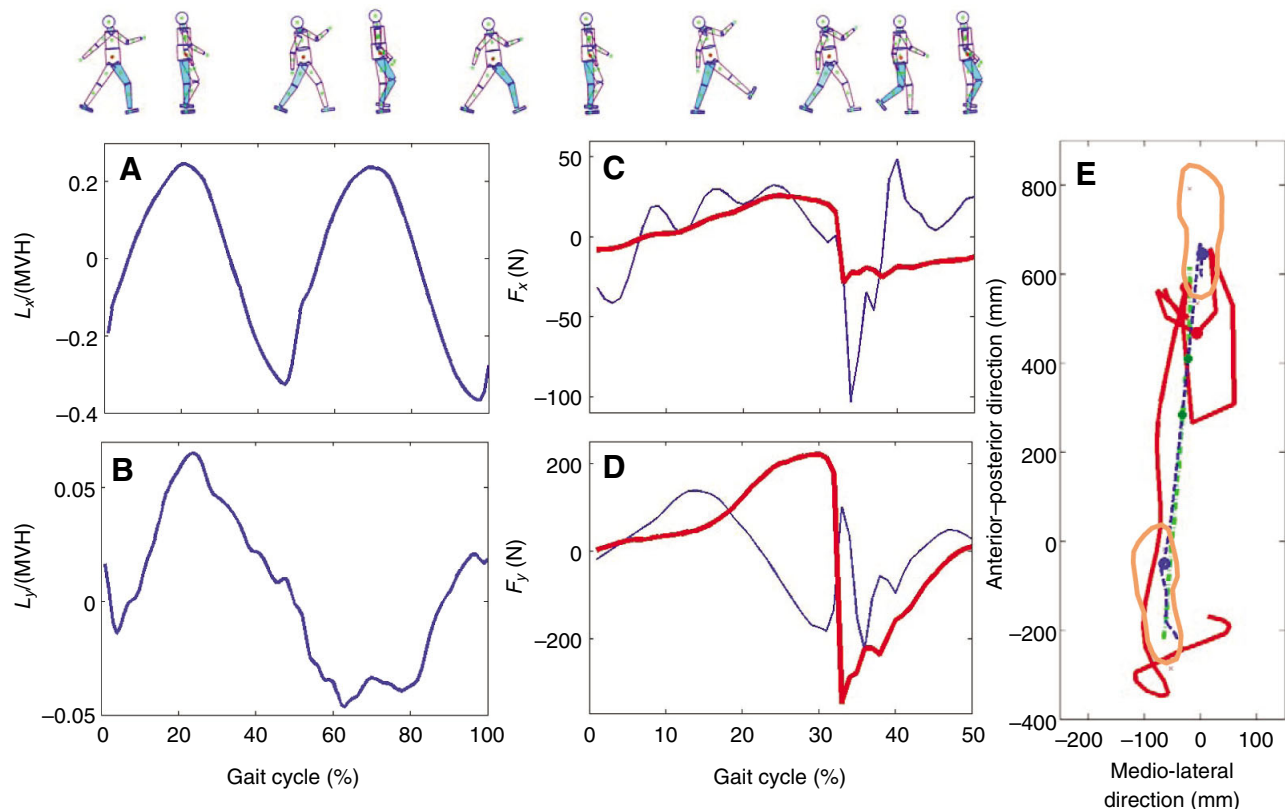
Fig. 9. Exaggerated walking gait. Angular momentum, horizontal ground reaction force and ground reference points are plotted in the medio-lateral (*x*) and anterior–posterior (*y*) directions. In this experiment a participant walked with exaggerated leg protraction and retraction movements, similar to a military marching gait, at a forward speed of 1.3 m s⁻¹ (see whole-body sketches above plots). (A,B) The horizontal components of normalized angular momentum are plotted *versus* percentage gait cycle. For ease of comparison with walking values shown in Fig. 3A, the angular momentum is normalized by the product of the participant's mass, CM height, and self-selected gait speed (*MVH*; see participant no. 1 in Table 1). Here 0% and 100% gait cycles correspond to consecutive heel strikes of the same foot. (C,D) The horizontal ground reaction forces measured experimentally (thin blue line) are plotted along with the calculated zero-moment forces (thick red line) *versus* percentage gait cycle for the same participant and trial as in A and B. Here 0% to 50% gait cycle spans from the middle of a single-support phase to the middle of the next single-support phase of the opposite limb. (E) Plotted are the CP (blue dashed line), CMP (red solid line) and CM ground projection (green dash-dotted line) trajectories and corresponding footprints. As in C and D, only 50% of the gait cycle is shown. The two circles on each line denote the transition from single to double support, and *vice versa*. For this exaggerated gait, the CMP often falls outside the ground support envelope.

What would be the benefits of a generalized strategy of angular momentum regulation in normal walking?

As highlighted in the last section, active generation of angular momentum is a key strategy for bipedal maneuverability and stability. Why then is momentum highly regulated during normal steady-state walking? To address this question, we conducted a second pilot study where a participant walked with exaggerated leg protraction and retraction movements, similar to a military marching gait, at a forward speed of 1.3 m s⁻¹ (see whole-body sketches above plots in Fig. 9). Kinetic and kinematic data were collected using the same experimental setup employed in the normal walking study, and the same human model was used for physical modeling. In Fig. 9, the angular momentum (Fig. 9A,B), horizontal ground reaction forces (Fig. 9C,D) and ground references points (Fig. 9E) are plotted in the medio-lateral (*x*) and anterior–posterior (*y*) directions. As with the hula-hoop motion, angular momentum is an order of magnitude larger than in normal walking (see Fig. 3A). Further, zero-moment forces do not agree well with experimental values ($R_x^2=0.01\pm0.12$; $R_y^2=-1.6\pm0.3$; mean±s.d. across seven gait trials), and the CMP diverges from the CP, often moving outside the ground support envelope ($\beta=50\pm6\%$).

The exaggerated walking plots of Fig. 9 clearly show that it is possible to walk with large CM moments. The dominant source of CM moment in this particular walking pattern is due to rapid body movements within the sagittal plane, as indicated by the large angular momentum values in the medio-lateral (*x*) direction (Fig. 9A) compared with the anterior–posterior (*y*) direction (Fig. 9B). Throughout much of the single-support phase, the swing leg protracts rapidly forward, often generating a positive CM moment in the medio-lateral (*x*) direction. As described by Eqn 9, this moment causes a positive moment force to act in the anterior–posterior (*y*) direction, accelerating the CM forward during early to mid-swing phase (see Fig. 9D). During terminal swing (18% to 30% gait cycle in Fig. 9D), the swing leg retracts towards the walking surface, generating a negative CM moment in the medio-lateral (*x*) direction and causing a negative moment force to act in the anterior–posterior (*y*) direction. This exaggerated retraction motion tends to decelerate the CM in the anterior–posterior (*y*) direction just prior to heel strike. Thus, throughout the single-support phase, the moment force tends to accelerate the CM forward as the result of swing-leg protraction, and then rapidly decelerate the CM as the swing leg retracts just prior to the double-support phase.

Walking in this manner, although possible from a stability standpoint, is nonetheless energetically expensive. Generating substantial CM moments by driving the swing leg in rapid protraction and retraction movements is likely to increase muscle work. The total kinetic energy increment resulting from body movements relative to the CM[6] (Willems et al., 1995) is 123±16 J (mean±s.d. across seven gait trials) for the exaggerated walk, a value that is 5-fold larger than the normal walking value from the same participant (22±2 J). Further, using the individual limbs method (Donelan et al., 2002), the positive and negative external work performed by the legs on the CM is 53±3 J and –40±6 J for the exaggerated walk, respectively. For normal walking from the same participant, the positive and negative external work is 28±2 J and –25±1 J, respectively. These preliminary results suggest that perhaps CM moments are kept small in normal steady-state walking in order to lower the body's work requirements, allowing for less muscle work and a more economical walking pattern.

The determinants of gait and segmental angular momentum cancellations

The gait determinants of pelvic rotation, controlled plantar flexion and powered plantar flexion are thought to be important mechanisms for making the CM trajectory flatter and smoother in walking (Saunders et al., 1953; Kerrigan et al., 2000; Kerrigan et al., 2001). Although pelvic obliquity and early stance knee flexion were also believed to produce flatter CM motions (Saunders et al., 1953), recent evidence suggests otherwise (Gard and Childress, 1997; Gard and Childress, 1999). We now discuss these particular determinants of gait in the context of segment-to-segment momentum cancellations. We found that feet and calf momenta are balanced by thigh momenta as a result of controlled plantar flexion, powered plantar flexion and early stance knee flexion, resulting in the relatively small medio-lateral (x) component of whole-body angular momentum. Further, we found that pelvis and abdomen momenta are balanced by segmental momenta from the rest of the body through the action of pelvic obliquity, resulting in the relatively small anterior–posterior (y) component of whole-body momentum. Finally, we show that leg angular momenta are balanced by segmental momenta from the rest of the body during pelvic rotation, producing the relatively small vertical (z) component of whole-body momentum.

Coronal plane rotational variability in normal human walking

Since steady-state walking comprises a series of coupled and alternating movement patterns, a reduced-order PC representation naturally exists for the high dimensional space of segmental angular momenta. For participant-independent PC analyses (using data from all participants and gait trials), we found that only three PCs are required to explain greater than 90% of angular momentum data in the medio-lateral (x) and vertical (z) directions, whereas four PCs are necessary in the anterior–posterior (y) direction. Furthermore, for participant-dependent analyses (using only individual participant data), we found that only three PCs are needed to explain greater than 90% of data about all three spatial directions (see Table 2).

In the anterior–posterior (y) direction, the fact that four PCs are required for a participant-independent analysis, and only three are

required for a participant-dependent analysis, highlights a more dominant rotational variability in the coronal (x–z) plane, across study participants, compared with sagittal and transverse planes. This result suggests that body dynamics that may be used to distinguish individual gait patterns in an angular momentum representation are mainly present in the coronal (x–z) plane. The specific source of the observed variability is predominantly due to large variations in the relative contribution of angular momentum in the abdomen and pelvis (segment 13), chest (segment 14) and head (segment 16) [see large standard deviations in Fig. 5 for PC_1 (y)].

In an analysis of passive dynamic walking stability, Kuo (Kuo, 1999) argued that bipedal walking is inherently unstable in the medio-lateral direction, and thus body movements within the coronal (x–z) plane would need to be actively controlled in order for the body to remain upright and stable. One interpretation of why there is a more dominant rotational variability in the coronal (x–z) plane is that distinct participant-dependent strategies are being expressed to achieve stable bipedal gait due to perhaps morphological variations between study participants. Although beyond the scope of the present study, the precise reason for the more dominant rotational variability in the coronal (x–z) plane is an interesting area for future research.

Future work

An understanding of angular momentum behaviors in human walking and other movement tasks may have important implications for several fields of study. In clinical gait research, the moment and zero-moment force components, as well as the CMP ground reference point, may potentially serve as valuable identification metrics for the diagnosis of pathological walking patterns such as was shown in Fig. 9. Further, in legged robotics research, an understanding of human angular momentum behaviors is likely to motivate improvements in humanoid controllers that effectively exploit both moment and zero-moment CM force components to improve robotic stability and maneuverability (Hofmann et al., 2004; Popovic et al., 2004b; Hofmann et al., 2007). It is our hope that this work will motivate further studies related to the biomechanics and control of human rotational behavior.

LIST OF SYMBOLS AND ABBREVIATIONS

$B_i(j)$	PC variability number: ratio between the area of the one sigma confidence interval of the normalized tuning coefficient $c_j^i(t)$ to the total area beneath the mean value curve
$c_j^i(t)$	Normalized tuning coefficients
$C_j^i(t)$	Time-dependent tuning coefficients
$\vec{D}(\alpha)$	A 16-component vector of segmental model densities
$\vec{D}^{Exp}$	A 16-component vector of mean segmental densities obtained from the literature
DE_j^i	Percentage of data (variance) explained with PC vector P_j^i
$D^i(\alpha)$	Density of the i-th segment
$\vec{F}$	Ground reaction force vector
$\bar{F}_{Exp}$	Grand mean, over all trials and gait percentages, of measured ground reaction force (x or y)
F_{Exp}^{ij}	j-th gait percentage of the i-th trial measured ground reaction force (x or y component)
F_{Mod}^{ij}	j-th gait percentage of the i-th trial model-predicted ground reaction force (x or y)
$F_{x,y}^{Moment}$	Horizontal components of ground reaction force corresponding to CM moment
$F_{x,y}^{Zero-moment}$	Horizontal components of ground reaction force corresponding to zero CM moment
G	Gravitational constant
$H_{subject}$	CM height

---

[6]This kinetic energy quantity was computed by taking the sum of the increments in the segment kinetic energy *versus* time curves of all the body segments relative to the CM. Willems et al. (Willems et al., 1995) argues that this kinetic energy quantity relates to the upper limit of internal mechanical work necessary to accelerate the limbs relative to the CM.

$\bar{\bar{I}}^i$	Segment i moment of inertia tensor about segment's CM
L	Angular momentum vector about the whole-body CM
m_i	Mass of the i-th segment
M_R	A 16-component vector of relative mass distribution throughout the model
M_R^{Exp}	A 16-component vector of mean relative mass values obtained from the literature
$M_i^R(\alpha)$	Relative mass of the i-th segment
$M_{subject}$	Total body mass
$M_{x,y}$	Horizontal moments measured relative to a fixed reference point on the force platform
N	Number of segments of human model, $N=16$
N_E	Number of PCs used for angular momentum cancellation estimate
$N_{Percent}$	Number of gait percentage times analyzed
$N_{subject}$	Angular momentum normalization constant
N_{Trial}	Number of trials
P_j^i	Principal component (PC) basis vectors, with $j=1\ldots3$ (spatial directions) and $i=1\ldots N$ (model segments or PCs)
P_j^{iq}	The angular momentum contribution of the q-th body segment to P_j^i
$\vec{r}_{CM}$	Whole-body CM position relative to lab frame
$\vec{r}_{CM}^i$	Segment i CM position relative to lab frame
$\vec{r}_{CMP}$	Centroidal moment pivot (CMP) receptor
$\vec{r}_{CP}$	Center of pressure location
R^2	Coefficient of determination
S_j	Segmental angular momentum cancellation in the j-th spatial direction
T	Moment vector about the whole-body CM
$\vec{v}_{CM}$	Whole-body CM velocity relative to lab frame
$\vec{v}^i$	The i-th segment's CM velocity relative to lab frame
V	Total body volume
V^i	Volume of segment i
V_R^i	Relative volume of the i-th segment
$\vec{V}_R$	A 16-component vector of relative volumes computed directly from the human model
$V_{subject}$	Walking speed
α	Parameter used in optimization of segment mass properties
α_{min}	Value of parameter α minimizing the absolute error $\lvert\vec{D}(\alpha)-\vec{D}^{Exp}\rvert$
$\beta\%$	Mean CP–CMP separation distance normalized by foot length
$_j$	A 16-component vector of segmental angular momenta in j-th spatial direction
^{i}	Segment i angular velocity vector about segment's CM

REFERENCES

Alexander, R. (1976). Mechanics of bipedal locomotion. In *Perspectives in Experimental Biology* (ed. P. S. Davies), pp. 493-504. Oxford, UK: Pergamon Press.

Bekker M. G. (1956). *Theory of Land Locomotion.* Ann Arbor: University of Michigan Press.

Cavagna, G. A., Thys, H. and Zamboni, A. (1976). The sources of external work in level walking and running. *J. Physiol. Lond.* **262**, 639-657.

Cavagna, G. A., Heglund, N. C. and Taylor, C. R. (1977). Mechanical work in terrestrial locomotion: two basic mechanisms for minimizing energy expenditure. *Am. J. Physiol.* **233**, R243-R261.

Croce, U. D., Riley, P. O., Lelas, J. L., and Kerrigan, D. C. (2001). A refined view of the determinants of gait. *Gait Post* **14**, 79-84.

Crowe, A., Schiereck, P., Boer, R. W. and Keessen, W. (1995). Characterization of human gait by means of body center of mass oscillations derived from ground reaction forces. *IEEE Trans. Biomed. Eng.* **42**, 293-303.

Dapena, J. (1978). A method to determine the angular momentum of a human body about three orthogonal axes passing through its center of gravity. *J. Biomech.* **11**, 251-256.

Dapena, J. (1993). An analysis of angular momentum in the discus throw. Paper presented at 14th International Congress of Biomechanics, Paris, France.

Dapena, J. and McDonald, C. (1989). A three-dimensional analysis of angular momentum in the hammer throw. *Med. Sci. Sports Exerc.* **21**, 206-220.

Donelan, M., Kram, R. and Kuo, A. (2002). Simultaneous positive and negative external mechanical work in human walking. *J. Biomech.* **35**, 117-124.

Dunn, O. J. (1964). Multiple comparisons using rank sums. *Technometrics* **6**, 241-252.

Elftman, H. (1939). The function of the arms in walking. *Hum. Biol.* **11**, 529-535.

Friedman, M. (1937). The use of ranks to avoid the assumption of normality implicit in the analysis of variance. *J. Am. Stat. Assoc.* **32**, 675-701.

Friedman, M. (1940). A comparison of alternative tests of significance for the problem of m rankings. *Ann. Math. Stat.* **11**, 86-92.

Frohlich, C. (1979). Do spring board divers violate angular momentum conservation? *Am. J. Phys.* **47**, 583-592.

Gard, S. A. and Childress, D. S. (1997). The effect of pelvic list on the vertical displacement of the trunk during normal walking. *Gait Posture* **5**, 233-238.

Gard, S. A. and Childress, D. S. (1999). The influence of stance-phase knee flexion on the vertical displacement of the trunk during normal walking. *Arch. Phys. Med. Rehabil.* **80**, 26-32.

Geyer, H., Seyfarth, A. and Blickhan, R. (2006). Compliant leg behaviour explains basic dynamics of walking and running. *Proc. R. Soc. Lond. B: Biol. Sci.* **273**, 2861-2867.

Goswami, A. and Kallem, V. (2004). Rate of change of angular momentum and balance maintenance of biped robots. Proceedings of the IEEE International Conference on Robotics and Automation, New Orleans, LA, USA, pp. 3785-3790. doi: 10.1109/ROBOT.2004.1308858, www.ieee.org.

Gu, W. (2003). The regulation of angular momentum during human walking. Undergraduate thesis, Physics Department, MIT, USA.

Herr, H., Hofmann, A. and Popovic, M. (2003). New horizons for orthotic and prosthetic technology: merging body and machine. Presented at the ZIF International Conference on Walking Machines, Bielefeld, Germany, http://biomech.media.mit.edu/publications/ArtificialMuscle_O&P.pdf.

Hinrichs, R. (1982). Upper extremity function in running. PhD thesis, The Pennsylvania State University, University Park, USA.

Hinrichs, R. (1987). Upper extremity function in running. II. Angular momentum considerations. *Int. J. Sport Biomech.* **3**, 242-263.

Hinrichs, R. (1992). Case studies of asymmetrical arm action in running. *Int. J. Sport Biomech.* **8**, 111-128.

Hinrichs, R., Cavanagh, P. and Williams, K. (1983). Upper extremity contributions to angular momentum in running. *Biomechanics VIII-B*. Champaign, IL, 641-647.

Hofmann, A. (2003). Control rules for biomimetic human bipedal locomotion based on biomechanical principles. PhD Thesis Proposal, Submitted to the Computer Science and Electrical Engineering Department, Massachusetts Institute of Technology.

Hofmann, A., Massaquoi, S., Popovic, M. and Herr, H. (2004). A sliding controller for bipedal balancing using integrated movement of non-contact limbs. IEEE/RSJ International Conference on Intelligent Robots and Systems, October, Sendai, Japan, pp. 1952-1959. doi: 10.1109/IROS.2004.1389683, www.ieee.org.

Hofmann, A., Popovic, M. and Herr, H. (2007). Exploiting angular momentum to enhance bipedal center-of-mass control. *IEEE Trans. Rob. Autom.* In press.

Jackson, J. (1991). *A User's Guide to Principal Components.* New York: John Wiley & Sons.

Kadaba, M. P., Ramakrishnan, H. K., Wooten, M. E., Gainey, J., Gorton, G. and Cochran, G. V. (1989). Repeatability of kinematic, kinetic, and electromyographic data in normal adult gait. *J. Orthop. Res.* **7**, 849-860.

Kadaba, M. P., Ramakrishnan, H. K. and Wooten, M. E. (1990). Measurement of lower extremity kinematics during level walking. *J. Orthop. Res.* **8**, 383-392.

Kerrigan, D. C., Croce, U. D., Marciello, M. and Riley, P. O. (2000). A refined view of the determinants of gait: significance of heel rise. *Arch. Phys. Med. Rehab.* **81**, 1077-1080.

Kerrigan, D. C., Riley, P. O., Lelas, J. L. and Della Croce, U. (2001). Quantification of pelvic rotation as a determinant of gait. *Arch. Phys. Med. Rehab.* **82**, 217-220.

King, D. (1999). Generating vertical velocity and angular momentum during skating jumps. Paper presented at 23rd annual meeting of the American Society of Biomechanics, University of Pittsburgh, October, 21-23, http://asbweb.org/conferences/1990s/1999/ACROBAT/086.PDF.

Kuo, A. (1999). Stabilization of lateral motion in passive dynamic walking. *Int. J. Robot. Res.* **18**, 917-930.

Kuo, A. D. (2002). Energetics of actively powered locomotion using the simplest walking model. *J. Biomech. Eng.* **124**, 113–120.

LeBlanc, M. and Dapena, J. (1996). Generation and transfer of angular momentum in the javelin throw. Proceedings of the 20th annual meeting of the American Society of Biomechanics. Atlanta, Georgia, USA, October 17-19, http://www.elitetrack.com/asbjavelin.pdf.

Lee, C. R. and Farley, C. T. (1998). Determinants of the center of mass trajectory in human walking and running. *J. Exp. Biol.* **201**, 2935-2944.

Margaria, R. (1976). *Biomechanics and Energetics of Muscular Exercise.* Oxford, UK: Clarendon Press.

McGeer, T. (1990). Passive dynamic walking. *Int. J. Robot. Res.* **9**, 62- 82.

Mochon, S. and McMahon, T. A. (1980a). Ballistic walking. *J. Biomech.* **13**, 49-57.

Mochon, S. and McMahon, T. A. (1980b). Ballistic walking: an improved model. *Math. Biosci.* **52**, 241-260.

Morasso, P. and Schieppati, M. (1999). Can muscle stiffness alone stabilize upright standing? *J. Neurophysiol.* **82**, 1622-1626.

Morasso, P., Baratto, L., Capra, R. and Spada, G. (1999). Internal models in the control of posture. *Neural Netw.* **12**, 1173-1180.

Ortega, J. D. and Farley, C. T. (2005). Minimizing center of mass vertical movement increases metabolic cost in walking. *J. Appl. Physiol.* **99**, 2099-2107.

Popovic, M., Gu, W. and Herr, H. (2002). Conservation of angular momentum during human locomotion. MIT, Artificial Intelligence Laboratory, Research Abstracts. September, 231-232, http://biomech.media.mit.edu/research/Popovic_Gu_Herr.pdf.

Popovic, M., Hofmann, A. and Herr, H. (2004a). Angular momentum regulation during human walking: biomechanics and control. Proceedings of the IEEE International Conference on Robotics and Automation. New Orleans, LA, USA, April, pp. 2405-2411. doi: 10.1109/ROBOT.2004.1307421, www.ieee.org.

Popovic, M., Hofmann, A. and Herr, H. (2004b). Zero spin angular momentum control: definition and applicability. IEEE-RAS/RSJ International Conference on Humanoid Robots. Santa Monica, CA, USA, November, www.ieee.org.

Popovic, M., Goswami, A. and Herr, H. (2005). Ground reference points in legged locomotion: definitions, biological trajectories and control implications. *Int. J. Robot. Res.* **24**, 1013-1032.

Portney, L. G. and Watkins, M. P. (2000). *Foundations of Clinical Research: Applications to Practice* (2nd edn). Upper Saddle River: Prentice Hall.

Riley, P., Krebs, D. and Popat, R. (1997). Biomechanical analysis of failed sit-to-stand. *IEEE Trans. Rehabil. Eng.* **5**, 353-359.

Rose, J. and Gamble, J. G. (1994). *Human Walking* (2nd edn). Baltimore, MD: Williams and Wilkins.

Saunders, J. B., Inman, V. T. and Eberhart, H. D. (1953). The major determinants in normal and pathological gait. *J. Bone Joint Surg. Am.* **35**, 543-558.

Simoneau, G. and Krebs, D. (2000). Whole-body angular momentum during gait: a preliminary study of non-fallers and frequent fallers. *J. Appl. Biomech.* **16**, 1-13.

Srinivasan, M. and Ruina, A. (2006). Computer optimization of a minimal biped model discovers walking and running. *Nature* **439**, 72-75.

Wilcoxon, F. (1945). Individual comparisons by ranking methods. *Biometrics* **1**, 80-83.

Willems, A., Cavagna, A. and Heglund, N. C. (1995). External, internal and total work in human locomotion. *J. Exp. Biol.* **198**, 379-393.

Winter, D. A. (1990). *Biomechanics and Motor Control of Human Movement.* New York: John Wiley & Sons.

Xu, D. and Wang, T. (1998). Lower extremity contributions to altering direction during walking: analysis of angular momentum. Proceedings of the North American Congress on Biomechanics. University of Waterloo, Waterloo, Ontario, Canada, August. http://asbweb.org/conferences/1990s/1998/160/index.html.